RESEARCH

Zinc oxide nanoparticles adsorb emerging pollutants (glyphosate pesticide) from aqueous solutions

Steven A. Odoemelam · Esther O. Oji · Nnabuk Okon Eddy · Rajni Garg · Rishav Garg · Saiful Islam · Mohammad Amir Khan · Nadeem A. Khan · Sasan Zahmatkesh

Abstract The present study captures the precipitation synthesis of zinc nanoparticles and modification with alumina and oleic acid. The crystalline size evaluated from the XRD profile of the zinc oxide nanoparticles was 18.05 nm but was reduced to 14.20 and 14.50 nm upon modification with oleic acid and alumina. The XRD spectra also showed evidence of the amorphous nature of zinc oxide nanoparticles and subsequent enhancement upon modification. A porous appearance was observed in the SEM instrumentation but seems to be enhanced by modification. The FTIR absorption spectra of the nanoparticles showed a peak associated with ZnO vibration around 449 cm, but the enhanced intensity was observed due to modification. The prepared ZnO-NPs and the modified samples were good materials for the adsorption removal of glyphosate from water, recording efficiencies above 94% at neutral pH and showing a possible incremental trend with an enhanced period of contact and adsorbent dosage. The adsorbents showed maximum capacity that ranged from 82.85 to 82. 97 mg/g. The adsorption models of Freundlich, Temkin, Dubinin–Radushkevich and BET showed excellent fitness. Results from computational results complemented experimental data and were used to identify the sites for adsorption and characteristics of molecular descriptors for the systems.

Keywords Emerging contaminants · Herbicide · Water · Toxicity reduction · Nano-adsorption

S. A. Odoemelam (✉)
Department of Chemistry, Michael Okpara University of Agriculture, Umudike, P.M.B. 7267 Umudike, Abia State, Nigeria
e-mail: saodoemelam@gmail.com

E. O. Oji
Department of Chemistry, Gregory University, Uturu, P.M.B 1012 Amaokwe Achara, Uturu, Nigeria

N. O. Eddy
Department of Pure and Industrial Chemistry, University of Nigeria, Nsukka, Enugu State, Nigeria

R. Garg
Department of Applied Sciences, Galgotias College of Engineering and Technology, Greater Noida, UP, India

R. Garg · M. A. Khan (✉)
Department of Civil Engineering, Galgotias College of Engineering and Technology, Greater Noida, UP, India
e-mail: amirmdamu@gmail.com

S. Islam
Civil Engineering Department, College of Engineering, King Khalid University, Abha-61421, Asir, Kingdom of Saudi Arabia

N. A. Khan
Interdisciplinary Research Center for Membranes and Water Security, King Fahd University of Petroleum and Minerals, Dhahran 31261, Saudi Arabia
e-mail: nadeem.khan@kfupm.edu.sa

S. Zahmatkesh (✉)
Tecnologico de Monterrey, Escuela de Ingeniería y Ciencias, Puebla, Mexico
e-mail: sasan_zahmatkesh@yahoo.com

S. Zahmatkesh
Department of Chemical Engineering, University of Science and Technology of Mazandaran, P.O. Box 48518-78195, Behshahr, Iran

Introduction

One of the major challenges of the global society is the lack of potable water or the increasing volume of waste and contaminated water (Warren-Vega et al., 2023). Consequently, the global society is currently stretching environmental, economic, industrial and domestic avenues to overcome the challenges arising from water contamination (Kumar et al., 2021). Some water contaminants have a short life span because they are biodegradable, but most contaminants that are nonbiodegradable or persistent are on the lists of emerging that should be given intensive research concerning remediation approaches because of their established toxicological documentation (Pérez-Lucas et al., 2023; Zahmatkesh et al., 2022)). Some emerging contaminants such as dyes, antibiotics, pesticides and other chemicals are useful in agricultural, scientific laboratories and several industrial sectors (Kaczorowska et al., 2023). This suggests that their production and availability are on the increase and point to the fact that increasing production, demand and supply should be adequately matched by remediation approaches (Silva et al., 2020; 2023).

One of the most vulnerable components of the environment that are worse impacted by the continuous discharg of toxic wastes is the aquatic environment because most contaminants are soluble in water and can easily be transported directly or indirectly to other components of the ecosystem (Caixeta, 2023). Consequently, research scientists around the globe have designed, tested and implemented several water treatment technologies (such as adsorption, ozonolysis, photodegradation, ion exchange, filtration, oxidation) to counter the forces of contamination (Sedighi et al., 2023). Pesticides are useful chemicals in the agricultural sector for the protection of crops against destruction, poor yield, food insecurity and associated economic and industrial problems (Hagner et al., 2019). Regardless of their utility or benefits, most pesticides (including glyphosate) are persistent in the environment and have an inherent tendency to be toxic to aquatic life, mainly when transported in solution to aqueous systems (Maderthaner et al., 2020). Some toxic impacts of glyphosate have been established and reported, including increased salivation, internal burns and cancer (Peillex and Pelletier, 2020). To remediate this impact, some laboratory-scale investigations have confirmed that among the available methods, an adsorption process is an excellent approach for the removal of toxic chemicals (including pesticide residue) from aqueous solutions (Odoemelam et al., 2018). Consequently, several conventional adsorbents have been established to be effective in the decontamination of water such as biochar showing removal efficiency of over 80% for atrazine, chlorothalonil and beta endosulfan from water (Kalsoom et al., 2022). Barbosa et al. (2023) also observed the effectiveness of sugar cane biomass as an adsorbent for the removal of fipronil from water with optimum removal efficiency exceeding 80%. The work of Naghdi et al. (2023) employed a porous metal–organic framework to remove glyphosate from water with an attended adsorption capacity of 440 mg/g, while Diel et al. (2022) observed efficiency approaching 90% with carbon nanotube as an adsorbent. Based on the above-reported work, there are some common challenges facing the selectivity, durability and efficiencies of adsorbents including irreducible particle size to enhance adsorption, the environmental requirement of non-constitution of primary or secondary contaminants, non-thermal stability, lack of structural information for enhanced modelling, inaccessibility, reusability and weak surface properties such as porosity and surface area (Gkika et al., 2022). Some of the listed shortcomings have impeded the economic cost of employing several adsorbents, especially at a commercial scale.

Of significant interest concerning the efficiency of an effective adsorbent is the requirement for minimal particle size and enhanced surface area (Cosgrove et al., 2022). Size modification below the micro-dimension may be impossible within the framework of most of the common adsorbents (Mazari et al., 2021). Therefore, the production of adsorbents with particle sizes of 1 to 100 nm (i.e. nanoparticles) can significantly boost adsorption capacity. Another challenge that concerns the water purification industry is the toxicity of some adsorbents, including some nano-adsorbents (Garg et al., 2021). For example, Hubbe (2022) and An et al. (2015) reported the toxicity of cellulose and jujube-based adsorbents and called for more intensive research attention towards managing the toxicity of the adsorbent. This implies that removing contaminants from water may be accomplished by the introduction of newer and foreign contaminants (Eddy et al., 2022a). As a result, long-term efforts must be made to find adsorbents that will not leach toxic components into the aqueous medium. Consequently, there is a current need

to design and apply eco-friendly adsorbents to remove pesticide residue (such as glyphosate) from the aquatic environment (Ghavamifar et al., 2023).

The International Union of Pure and Applied Chemistry (IUPAC) nomenclature for glyphosate is ((3-hydroxy-2-oxopropyl) amino) methyl phosphonic acid. It is an active and standard ingredient in most pesticides, and its commercial value is highly appreciable because of its outstanding effectiveness as a pesticide (Diel et al., 2022). The toxicity of this product has been confirmed, especially its impact on body weight, skeletal composition, gastrointestinal systems and initiation of cancer and death (Tarazona et al., 2017). Unfortunately, this toxic compound can easily be ingested through contaminated food, drinking water and other routes (Da'ana et al., 2021). It can equally affect the aquatic environment through a reduction in primary productivity (and a retardation of the amount of light penetrating the water and subsequent retardation of photosynthesis), nutrient enrichment and the termination of the aquatic population (Peillex & Pelletier, 2020). Given the closeness of the contamination route of glyphosate, its common usage, its toxicity and the need to employ eco-friendly adsorbents for their removal, our current study is aimed at the employment of the precipitation method to synthesize, modify, characterize and apply zinc oxide nanoparticles (ZnO-NP) to eliminate glyphosate from aqueous solution. The chemical structure of glyphosate is shown below.
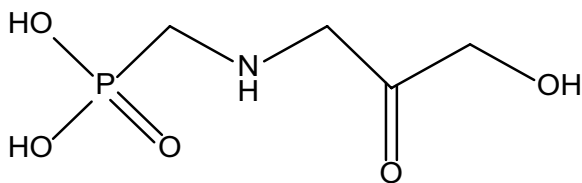
The structure suggests some inherent tendency of the compound towards adsorption based on the presence of heteroatoms (O, N and P), adsorption-prone functional groups and pi-electrons (Eddy et al., 2022b).

The success of zinc nanoparticles rather than zinc oxide nanoparticles has also been reported for the removal of glyphosate residue from contaminated water with recorded optimum efficiency of 70%. However, zinc nanoparticles can be very reactive with some contaminants, unlike zinc oxide nanoparticles which are relatively stable (Al-Arjan, 2022). This suggests that
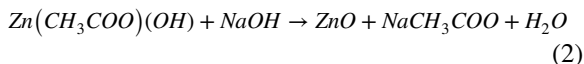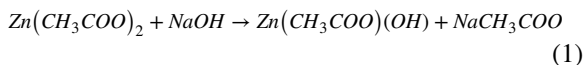
the generation of secondary contamination is more feasible with ZnNPs than ZnO-NPs. Some studies have also shown that the adsorption capacity of nanoparticles such as ZnO-NPs can be enhanced through doping or capping with other compounds. For example, Hosseini and Toosi (2019) observed that graphene–titanium oxide nanocomposites yielded removal efficiency extending from 53 to 73% for some herbicides (including 2,4-D, glyphosate compared to TiO$_2$ or graphene that showed efficiency not exceeding 48%. The only literature on the viability of zinc oxide nanoparticles (ZnONPs) as an adsorbent for glyphosate is the one reported by Páez et al. (2019). Their work indicated that ZnO-NPs were synthesized by precipitation methods and applied in the removal of glyphosate-based herbicides from water. The efficiency describing the adsorption removal technology assumes an optimum value of about 90%. The study showed some merit in the application of the nanoparticles and also opens room for further modifications that can thrive towards the enhancement of efficiency; some are the investigation of environmental variables affecting the observed adsorption, the stabilization of the adsorbent by doping and the establishment of the theoretical or computational chemistry descriptors that can be useful in the prediction of future adsorption descriptors and other structure-based predictors. Therefore, in this study, we are consolidating the research need for the enhancement of the adsorption capacity of ZnO-NPs through doping as a predictor for better adsorption removal of the toxic herbicide, which is popularly used in several countries of the world including Nigeria and India. The investigation of environmental variables that can affect the adsorption characteristics of the ZnO-NPs as well as the establishment of theoretical based descriptors is also incorporated into the work and shall form the baseline information for the first time.

Materials and methods

Sample preparation and synthesis

All chemicals were purchased from BDH Limited, Poole, England, and Aldrich Company, Germany. The chemicals were used as delivered and without further purification. The precipitation method described by Mohan and Renjanadevi (2016) was adopted for synthesizing the ZnO-NP using zinc acetate dehydrate

and NaOH as precursors. The first stage of the reaction involves the production of sodium acetate and zinc hydroxide acetate (Eq. 1). In contrast, the second stage involves further interaction of the zinc hydroxyl acetate and sodium hydroxide (Eq. 2) to produce ZnO:

$$Zn(CH_3COO)_2 + NaOH \rightarrow Zn(CH_3COO)(OH) + NaCH_3COO \tag{1}$$

$$Zn(CH_3COO)(OH) + NaOH \rightarrow ZnO + NaCH_3COO + H_2O \tag{2}$$

The synthesized zinc oxide nanoparticles were washed with deionized and distilled water severally and filtered with a Whatman No. 1 filter paper. It was washed with 20 ml of 96% ethanol and dried in an oven at 100 °C for 4 h before calcination. A portion of the prepared zinc oxide nanoparticles was modified using oleic acid and xylene, as described by Hong et al. (2006). The remaining portion was also modified with aluminium oxide as described by Yuan et al. (2005).

To prepare stock solutions of glyphosate, 1 g of the pesticide was dissolved in 1000 ml of distilled water to achieve a concentration of 1000 mg/L. Using a UV/VIS 1800 PC spectrophotometer, a calibration curve was developed using various working concentrations (2, 3, 4, 4.5 and 6.5 mg/L) prepared from the stock solutions.

Adsorption removal techniques

According to Yuan et al. (2005), batch adsorption experiments were conducted using 10 mg/L pesticide solutions (except for experiments investigating the effects of initial concentration, in which different concentrations were used: 2.0, 3.0, 4.0, 4.5 and 6.5 mg/L. Each analysis used 0.6 g of adsorbent, except for the study that investigated the effects of adsorbent dosage, which used various adsorbent masses (0.1, 0.2, 0.4 and 0.6 g) and a fixed pesticide concentration (10 m/g).

A UV/VIS 1800 PC spectrophotometer was used to measure absorbance to determine the amount of pesticide adsorbed and the difference between the initial (inlet) concentration and the equilibrium concentration (after adsorption, i.e. $C_0 - C_e$ was recorded as the amount of pesticide adsorbed. C_0 is the initial concentration, while C_e is the concentration at equilibrium. The percentage concentration of pesticide removed was calculated using Eq. 3, while the equilibrium amount of pesticide adsorbed was evaluated using Eq. 4 (Ali et al., 2022):

$$\%Removal = \frac{C_0 - C_e}{C_0} \times \frac{100}{1} \tag{3}$$

$$Q_e = \frac{C_0 - C_e}{C_0} \times \frac{m}{V} \tag{4}$$

where m is the mass of the adsorbent used for the study and V is the volume of the solution

Characterization of ZnO-NP

The Fourier transformed infra-red spectrum (FTIR) of the ZnO-NPs was obtained by scanning the sample in a FTIR instrument (Shimadzu FTIR-54005) between the wave number of 4000 and 400 cm^{-1}. The spectrum obtained was presented as peaks of absorbance against wave number. The ZnO-NPs were also characterized using the XRD (model PANalytical X'Pert Pro) which operated at a voltage peak of 45 kV and a regulated current of -35 mA. The operation also employed a Cu–Kα radiation (K = 1.5406 A°) and 2θ ranging from 20 to 80° at a continuous speed of 0.045° per min. The morphological analysis of the nanoparticles was implemented using a scanning electron microscope (Model JEOL JSM6100) with an accelerating voltage of 20 kV after super coating within a layer of gold.

Quantum computation

ChemBio version 18 was used to draw chemical structures. Optimization of the drawn chemical structures was done using DFT models in the Materials Studio program, which was also the software used in the computation of the Fukui function through Mulliken and Hirshfeld charges (Q). The DFT/B3LYP/6-311G** level of theory was used for the calculations of semiempirical parameters such as frontier molecular orbital energies, total molecular energy and dipole moment. The adsorption energy and associated energy functions such as rigid adsorption energy, deformation energy and others were obtained through Monte Carlo simulation modelling positioned as an adsorption locator in the Materials Studio program.

Results and discussion

Characterization of the synthesized ZnO-NP

Figure 1 shows the scanning electron micrographs (SEM) of (a) ZnO-NPs, (b) ZnO-NPs modified with alumina and
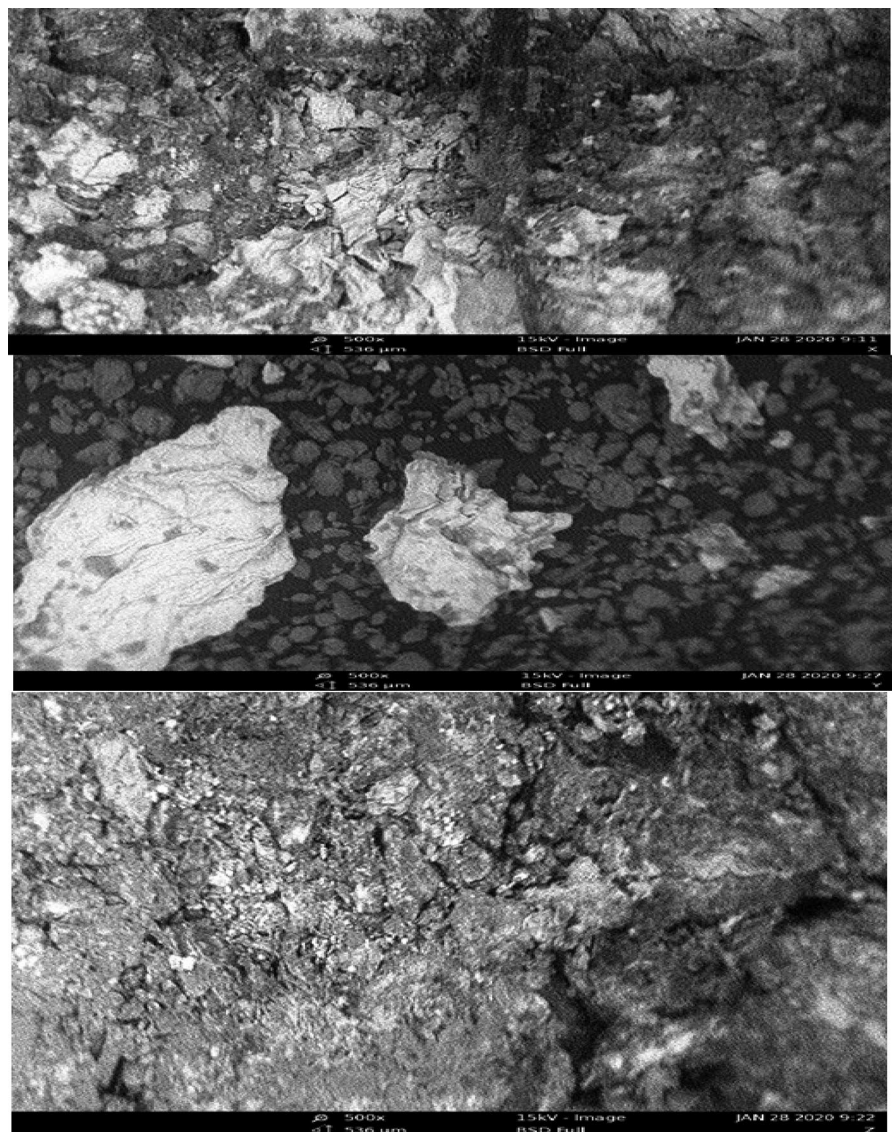
(c) ZnO-NPs modified with oleic acid and xylene. The micrographs were obtained based on the resolution (500×) indicated in each figure. The examination of the micrographs (Fig. 1) reveals that the modification changed the morphology of the ZnO-NPs. The unmodified micrograph reveals less clumsiness in the nanoparticles. However, modification with alumina reveals more evenly arranged spherical particles within the exclusive and relatively broad adsorptive sites with different morphological appearances, at the bottom left (largest diameter), centre (average diameter) and top right (most minor diameter).

Also, the ZnO-NPs modified with oleic acid and xylene gave a relatively better and more ordered morphology than the unmodified ZnO-NPs. From the appearance or morphology of the three micrographs, there is a development of a more ordered and defined structured appearance that can be attributed to modification. Some reports have been documented on the morphology of nanoparticles after modification. For example, Egbuchunam and Balkose (2012) observed that ZnO-NPs consisted of spherical particles and were monodisperse, but modification with inorganic compounds increased aggregation.

In the work of Mohan and Renjanadevi (2016), the morphology of ZnO-NPs synthesized showed a grain-like and spherical appearance, while Kamal et al. (2023) reported a hexagonal shape for ZnO-NPs.

Fig. 1 Scanning electron micrographs of **a** ZnO-NP, **b** MAlO and **c** MOLA

The X-ray diffraction spectra of the ZnO-NPs, ZnO-NPs modified with alumina (MAlO) and ZnO-NPs modified with oleic acid (MOLA) are shown in Fig. 2a to c, respectively. The XRD spectra (Fig. 2) reveal sharp peaks for crystalline ZnO-NPs with a hexagonal wurtzite structure, consistent with the range of values reported elsewhere (Xin, 2022). The observed sharp peaks indicate an excellent crystallinity of the ZnO-NP at $2\theta = 8.4874°$, $12.6734°$, $16.5172°$, $28.4438°$, $33.0871°$ and $59.3223°$, while the rough surface indicates the amorphous areas with relatively broad peaks.

According to Zhou et al. (2017) and Khoshhesab et al. (2011), the diffraction peaks at $33.0871°$ and $59.3223°$ are associated with the hexagonal wurtzite phase of ZnO. Peaks at 8.4874, 12.6734 and 16.5172 indicate the presence of $Zn(OH)_2$ and ethanol in the drying process. A reduction in peak intensity (but an increase in the number of peaks) of ZnO-NPs was observed due to the inclusion of aluminium oxide (Fig. 2b), which contributed to the increase in the amorphous character of the ZnO-NPs (Gogoi et al., 2020). However, the peaks are much broadened, and the crystallinity of ZnO-NPs tends to decrease, while peaks were observed at $2\theta = 31.1748°$ to $67.3585°$. On the other hand, the weak crystallinity of the ZnO-NPs after oleic acid inclusion occurred at $2\theta = 33.0113°$ (fig. 2c).

In view of the diffraction peaks observed for the nanoparticles, significant information can be obtained from the XRD spectrum regarding nanoparticle dimension through the application of the Scherrer equation given as Eq. 5 (Hong et al., 2006):

$$Crystalline\ size(nm) = \frac{k\lambda}{Bcos\theta} \qquad (5)$$

Fig. 2 XRD spectra of (a) ZnO-NP, (b) MAlO (ZnO-NPmodified with alumina) and(c) MOLA (ZnO-NP modified witholeic acid and xylene)
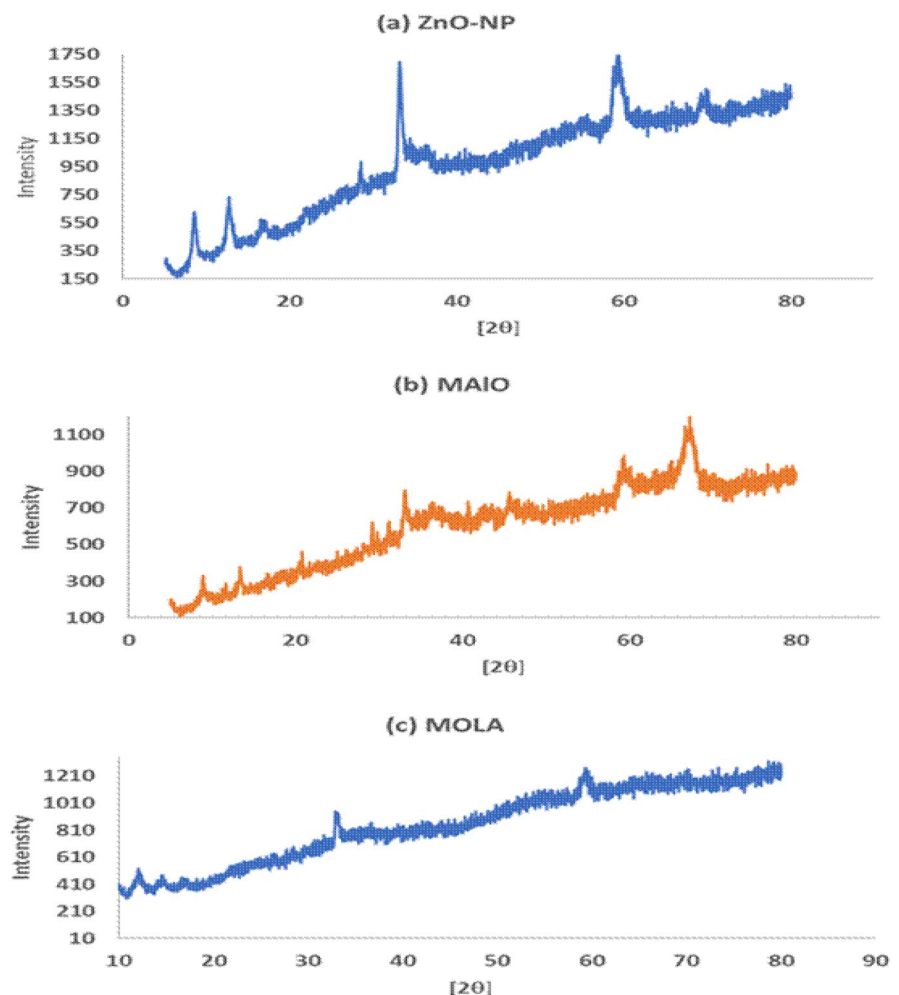
where k is Scherrer's constant ($k = 0.94$ for spherical crystallites with cubic symmetry), λ is the wavelength of the X-ray, β is the full width at half maximum of the XRD peak and θ is the diffraction angle, deduced from the XRD peak position, i.e. 2θ.

The crystallite sizes of the unmodified nanoparticles were estimated as 32.25, 18.79, 7.35, 16.39, 8.48 and 7.01 nm, which gave an average of 18.05 nm. Also, the crystallite sizes of the MOLA were 18.27, 14.20, 22.98, 9.65 and 5.90 nm (average = 14.2 nm). A similar trend was observed for the MAlO, whose corresponding crystallite sizes were 46.0, 31.13, 7.04, 21.43, 10.26, 11.84, 4.69, 6.71, 4.35 and 5.53 nm (average = 14.50 nm). The peaks around 33.0871 and 59.3222° are typical for the wurtzite structure of ZnONPs (Pelicano et al., 2017).

The analysed XRD data also confirmed that the modification of ZnONPs with alumina changes the peak at 33.0871 to 33.1362°, while the peak at 59.3222° is absent in the modified ZnO-NPs. Relatively new peaks were formed at 20.24, 29.24, 3.17, 36.39, 40.72, 45.62 and 61.35°. However, modification with oleic acid changes the peak from 33.09° to 33.01°, while the original peak of 12.65° was changed to 12.07°. The increase in the number of peaks (and their broadness) due to alumina and oleic acid modification makes the ZnO nanoparticles less crystalline (and more amorphous) (Zhao et al., 2021). It can be seen from the XRD spectrum that the modification with alumina tends to increase the crystallite size and the number of peaks more than what was found in the ZnO-NPs. In contrast, modification with oleic acid reduces the number of peaks and the particle sizes of the nanoparticles. Also, the alumina tends to make the ZnO-NP more ordered, while the oleic tends to increase the crystallinity of the synthesized nanoproduct. There were also observable changes in peak intensities after the modifications, showing a slight decrease for alumina-modified ZnO-NPs and an increase for the oleic acid-modified ZnO-NPs.

Figure 3 shows the FTIR spectra of the ZnO-NPs, MAlO and MOLA. Figure 3 shows the FTIR spectra of glyphosate, MAlO, MOLA and ZnO-NPs. The spectra reveal a general observation concerning the nanomaterials: enhanced absorption due to modification with alumina (MalO) and oleic acid (MOLA). The FTIR of glyphosate (Fig. 3) reveals OH stretches at 922 and 12,630 cm^{-1}, PO$_2$ stretches at 1198 and 1087 cm^{-1}, CO stretches at 1745 cm^{-1}, and NH2 stretches at 1600 cm^{-1}. Also, the FTIR spectrum of ZnO-NP indicated the presence of vibration due to ZnO at 479 cm^{-1} and hydroxyl stretches at 3572, 3467, 3549 and 3467 cm^{-1} (Dangana et al., 2023), possibly due to traces of NaOH and H$_2$SO$_4$ that were used for the preparation (Handore et al., 2014).

O=C=O stretches were observed at 2348 and 1030 cm^{-1} (Hong et al., 2021), and C=C stretch was observed at 1598

Fig. 3 FTIR spectra of glyphosate (GLY), ZnO-NPs, ZnO-NPs modified with alumina (MAlO) and ZnO-NP modified with oleic acid and xylene (MOLA)
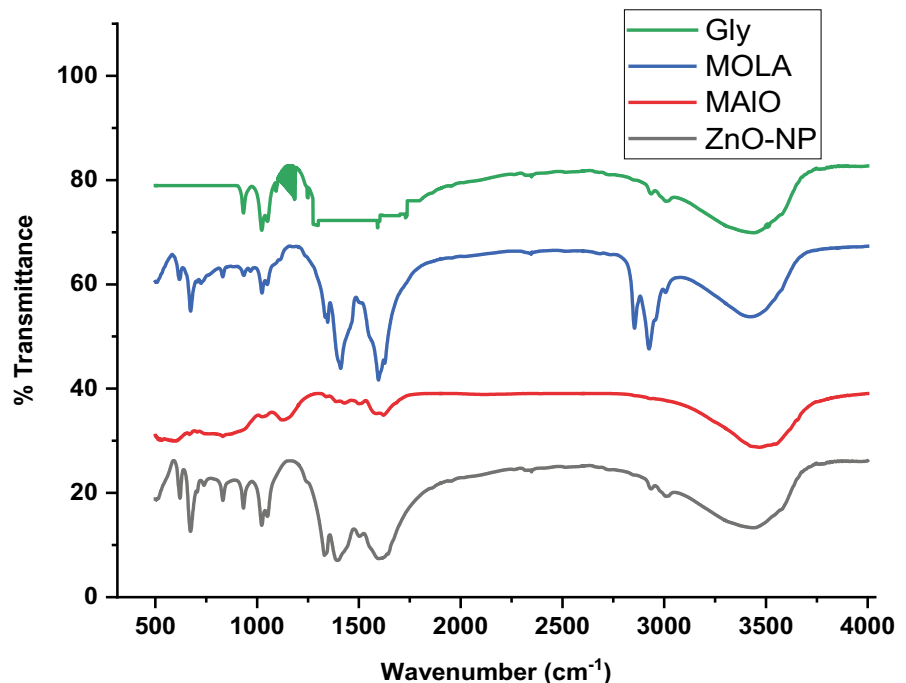
and 831 cm^{-1}. C-O stretches were observed between 1022 and 1123 cm^{-1} (Tiwari et al., 2022). These stretches might have resulted from traces of unreacted acetate ions. However, after adsorption of the pesticide, the OH stretches at 3572 and 3439 cm^{-1} were shifted to 3536 and 2501 cm^{-1}, respectively, while the functional groups at 3467 and 3549 cm^{-1} were shifted to 3463 and 3422 cm^{-1}, respectively. These changes indicate the interaction between the ZnO-NP and the glyphosate. Also, new OH stretches were formed at 3881, 3866, 3803, 3746 and 3646 cm^{-1}, indicating the involvement of these bonds in adsorption. The C-O, C=C and C-H stretches were not found in the spectra of the adsorbent after adsorption, which also suggests their interaction and subsequent involvement in bond formation.

After modification of the adsorbent with oleic acid, the FTIR of MOLA reveals almost similar functional groups but at different positions, including OH stretch at 3421 cm^{-1} but not at 3572, 3467, 3549 and 3467 cm^{-1} that were found in ZnO-NPs. This OH stretch was shifted to 3536 cm^{-1}, contrary to the multiple stretches in ZnO-NPs. The observed difference may be partly attributed to the reducing action of oleic acid. C-O stretch at 1025 cm^{-1} was missing a functional group. However, new C-O bonds were formed at 1455 and 1404 cm^{-1} indicating their involvement in adsorption. After the glyphosate adsorption, the C-H bond at 984 cm^{-1} and the O=C=O stretch were also missing in the MOLA spectra. Some of the newly introduced vibrations might have been introduced by the adsorbed glyphosate, for example, NH$_2$ stretches.

The MAlO FTIR spectrum after the adsorption of glyphosate revealed multiple OH stretching (at 3646, 3463, 3422, 3881, 3866, 3803, 3463 and 3422 cm^{-1}) as shown in the results, which suggest the relative contribution of OH stretching in the adsorption of the glyphosate. The OH stretches must have been due to those from the glyphosate and the adsorbents. However, the C-H stretches (at 1499 and 1429 cm^{-1}) and the C-O stretch (at 11,322 cm^{-1}) were missing in the spectrum of the adsorbent after the adsorption of glyphosate, which also confirmed their involvement in the adsorption process.

It is also evident from the results presented that some functional groups were missing after adsorption, while others experienced changes in the frequency of adsorption. Also, new functional groups were formed. The observed changes and modifications are evidence of interaction and adsorption through the employment of functional groups, as reported elsewhere (Eddy et al.,

2022c). For example, the reported stretches at 3572 and 3472 cm^{-1} in ZnO-NP shifted after adsorption shifted to 3536 and 3501 cm^{-1}, respectively. The O=C=O stretch at 2348 cm^{-1} in the ZnO-NPs was not found in the FTIR spectrum of the adsorbent (ZnO-NPs) after adsorption. Multiple OH stretches formed new bonds (3881, 3866, 3803, 3746 and 3646 cm^{-1}). These new bonds were probably used in the glyphosate adsorption onto the ZnO-NPs. The employment of MAlO and MOLA as adsorbents for the removal of glyphosate from water also reveals some frequency shifts, the disappearance of bonds and the formation of new bonds.

Batch adsorption study

Results showing the variation in the amount of glyphosate adsorbed with some analytical parameters such as time, concentration and adsorbent dosage are displayed in Fig. 4. The adsorbent dosage was found to exert a positive impact on the adsorption of glyphosate by the three adsorbents (Fig. 4a), such that the equilibrium amount of glyphosate adsorbed experienced a rise with an increase in the mass of the adsorbent. Literature has shown that an increase in the mass of the adsorbent generally results in improved adsorption because there is a corresponding increase in the number of active adsorption sites. Therefore, as more adsorbate molecules diffuse to the surface, the vacancy for further adsorption would be enhanced (Elfeky et al., 2020). These results also align with the findings reported by Naghdi et al. (2023) for the adsorption removal of glyphosate by the metal–organic framework.

The best adsorption tendency regarding the period of contact was achieved by the unmodified sample (i.e. ZnO-NPs), while the MAlO exhibited the least. This may be related to the nature of porosity and the tendency of the adsorbent to be relatively weakened as the contact period increases (Fig. 4b). Some studies have given explanations on possibilities that favours the mutual increment in adsorption and time concerning the adsorption of organic molecules. Some attributed such observations to the successful equilibration of the adsorbate–adsorbent system, which is principally dependent on time as explained in this context (Silva et al., 2020). The period of contact of the adsorbate with the adsorbent in the solution was also observed to affect the extent of adsorption of glyphosate pesticides such that as the contact period increases, more of the adsorbate molecules had the opportunity to be adsorbed
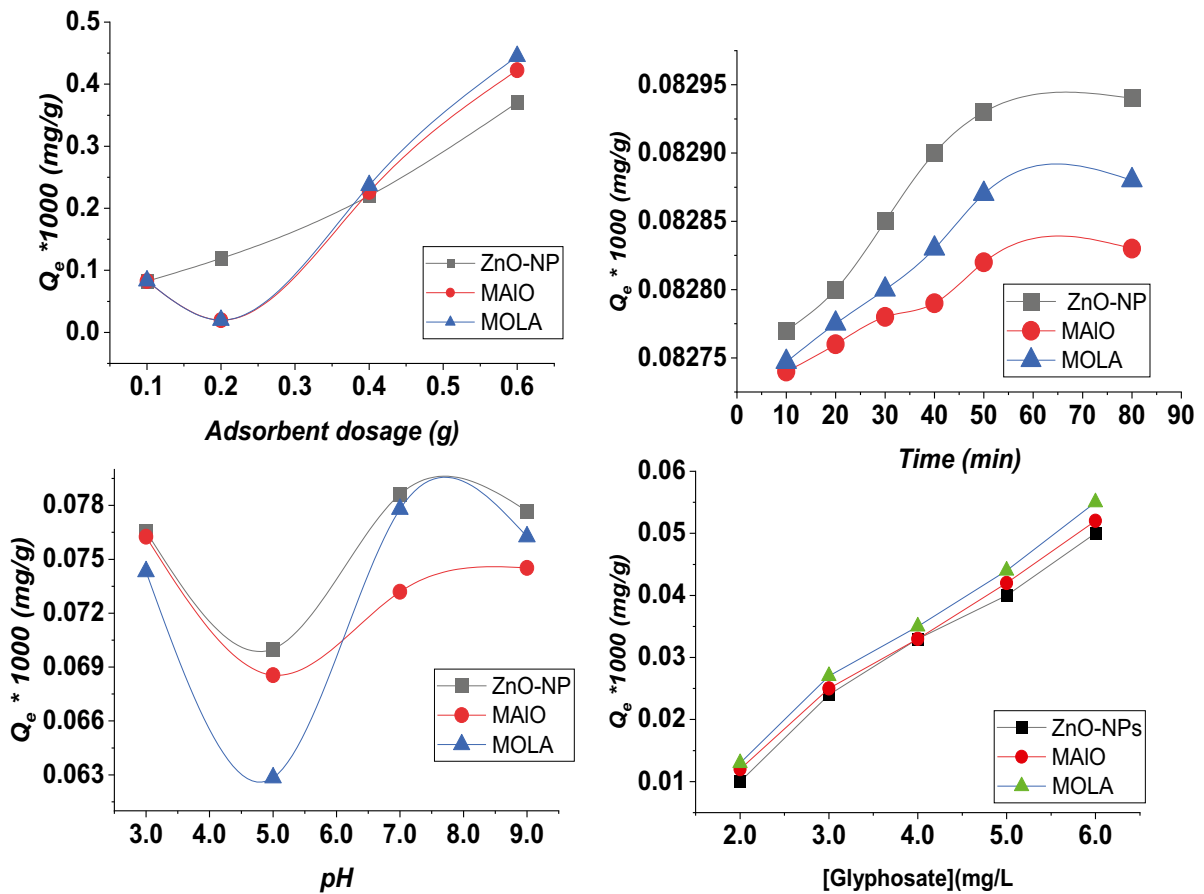
Fig. 4 Variation of equilibrium amount of glyphosate adsorbed by ZnO-NPs, MAlO and MOLA with adsorbent dosage, pH and initial concentration of glyphosate

due to enhanced interaction between the adsorbed species and the penetration power of the adsorbate towards the electric double layer as the contact period increases. A similar trend in variation of the amount of glyphosate adsorbed with time was observed and reported by Sen and Mondal (2022) and Chen et al. (2016) for the adsorption of glyphosate from an aqueous solution by some non-ZnO-NP adsorbents.

Between the pH of 3 and 5 (Fig. 4c), the equilibrium amount of glyphosate adsorbed decreases by 7.67%, 7.87% and 13.77% for ZnO-NPs, MAlO and MOLA, respectively. Consequently, the highest decrease in adsorption was observed for the MOLA adsorbent. The decreasing trend was followed by a sharp increase that resulted in comparable efficiencies for both ZnO-NPs and MAlO. The two adsorbents also seem to display similar adsorption mechanisms (as shown by the parallel pattern recorded for the adsorption profiles of the two adsorbents for glyphosate).

However, at a pH of 9, ZnO-NPs had the best adsorption efficiency (% Removal=93.27%), while MAlO had the lowest, and MOLA had the highest (% Removal=93.27%). At a pH of 9, the recorded efficiency was 91.54%.

The optimum pH for the removal of the pesticide was 7, 3 and 7 for ZnO-NP, MAlO and MOLA, respectively. That means the removal of MAlO is best favoured at an acidic while profiles the dominance of H^+. This may be ascribed to the fact that Al_2O_3 (though amphoteric) causes the ZnO-NPs to act as a base and thus exert a strong affinity for the adsorption at acidic pH (Pereira et al., 2019). The dependent pH for the other adsorbents witnessed the best conditions at neutral pH. The observed trend is not strange when considering the available literature. For example, Mattos et al. (2017) also reported a pattern similar to the observation in this study while investigating the variation of glyphosate adsorption with pH.

An increase in the initial concentration of the adsorbate (Fig. 4d) was also found to produce an increase in adsorption because more molecules are available to compete for the available adsorption sites (Al-Harby et al., 2021). It is certain that as long as the available adsorption sites have not been saturated, the tendency for an adsorbent to accommodate more adsorbate molecules will increase with an increase in concentration. At lower concentrations, once the adsorbate molecule is unable to diffuse to the adsorbent surface, adsorption will decrease, but at higher concentrations, there would be enough molecules to compete for the adsorption sites (Rápó & Tonk, 2021). The kinetics of the adsorption process was investigated through the fitting of experimental data into pseudo-first-order, pseudo-second-order, Weber–Morris and Elovich kinetic models, which are described by Eqs. 6 to 9, respectively (Babapour et al., 2022):

$$ln\left(Q_e - Q_t\right) = lnQ_e - k_1 t \qquad (6)$$

$$\frac{t}{Q_t} = \frac{1}{k_2 Q_e^2} + \frac{t}{Q_e} \qquad (7)$$

$$Q_t = k_{id} t^{1/2} + C_{id} \qquad (8)$$

$$Q_t = \frac{1}{\beta} ln(1 + \beta\alpha t) = \frac{1}{\beta} ln\beta\alpha + \frac{1}{\beta} lnt \qquad (9)$$

The suitability of a pseudo-first-order model to the adsorption of glyphosate by ZnO-NP, MAlO and MOLA was investigated by plotting against time (based on Eq. 6). The linear plot (plots not shown) obtained gave the best R^2 value for MALO (Table 1). The values of the theoretical equilibrium amount of the pesticide adsorbed (Q_e) were low, but the ZnO-NP gave the closest approximation to the experimental data. The highest pseudo-first-order rate constant was exhibited by MOLA and the least by MAlO, indicating the adsorption becomes faster in that order. However, perfect correlations ($R^2 = 1$) were obtained for the three adsorbents (Table 1) through the pseudo-second-order plots (Fig. 5) compared to the pseudo-first-order model, which gave R^2 values (ranging from 0.8316 to 0.9314) that are relatively lower than those calculated for pseudo-second-order. Excellent approximation was also observed for the theoretical equilibrium amount of glyphosate adsorbed (ranging from 82.85 to 82. 97 mg/g) compared to the experimental average of 82.90 mg/g

(Table 1). Therefore, the kinetics of the adsorption process is best described by the pseudo-second-order model. Others have published similar deductions concerning the adsorption of glyphosate by various adsorbents and accepted the pseudo-second-order kinetics as best fitted (Jia et al., 2011). Therefore, the adsorption rate is majorly limited by chemisorption and not solely by diffusion (Bazan-Wozniak & Pietrzak, 2023).

The linear plot describing the intraparticle diffusion model (Fig. 5) did not give a zero intercept, confirming that the adsorption is not limited by diffusion (Xu et al., 2022). The estimated rate constant (Table 1) was the highest for the adsorption of glyphosate by ZnO-NPs and MOLA, which is consistent with the inference drawn from the pseudo-second-order models (Table 1). The application of the intraparticle diffusion model to the adsorption removal of glyphosate by calcined calcium aluminium hydrotalcite has also been affirmed by Peng et al. (2021).

The Elovich model was also accepted since a plot of Qt against t was linear as shown in Fig. 5. From the model, the constants a and b have mgg^{-1} min^{-1} and $g.mg^{-1}$ as their respective units. The initial rate was the highest for MOLA and lowest for ZnO-NPs, which is the inverse of the constant rate values obtained from the other models.

The Elovich model predicts that ZnO-NPs have the least initial adsorption rate but the least desorption rate,

Table 1 Evaluated kinetic parameters for the adsorption of glyphosate by ZnO-NPs, MAlO and MOLA

	ZnO-NP	MAlO	MOLA
Pseudo-first-order			
R^2	0.8966	0.8366	0.9314
Q_e (mg/g)	0.000488	0.000184	0.001207
K_1 min^{-1}	0.0692	0.0495	0.0888
Pseudo-second-order			
R^2	1.000	1.000	1.0000
Q_e (mg/g)	82.974	82.85	82.953
K_2 min^{-1}	0.015974	0.028189	0.009126
Elovich			
R^2	0.9369	0.947	0.9503
β	11,111.11	14,285.71	20,000
ln (a)	907.351	1170.433	1642.097
Weber–Morris			
R^2	0.9134	0.9547	0.9841
k_{id} (min^{-1})	0.00000053	0.0000002	0.00000003
C_{id}	0.0827	0.0827	0.0827

Fig. 5 Pseudo-first-order plots for the adsorption of glyphosate by ZnO-NP, MAlO and MOLA and Webber–Morris and Elovich isotherms for ZnO-NP, MAlO and MOLA
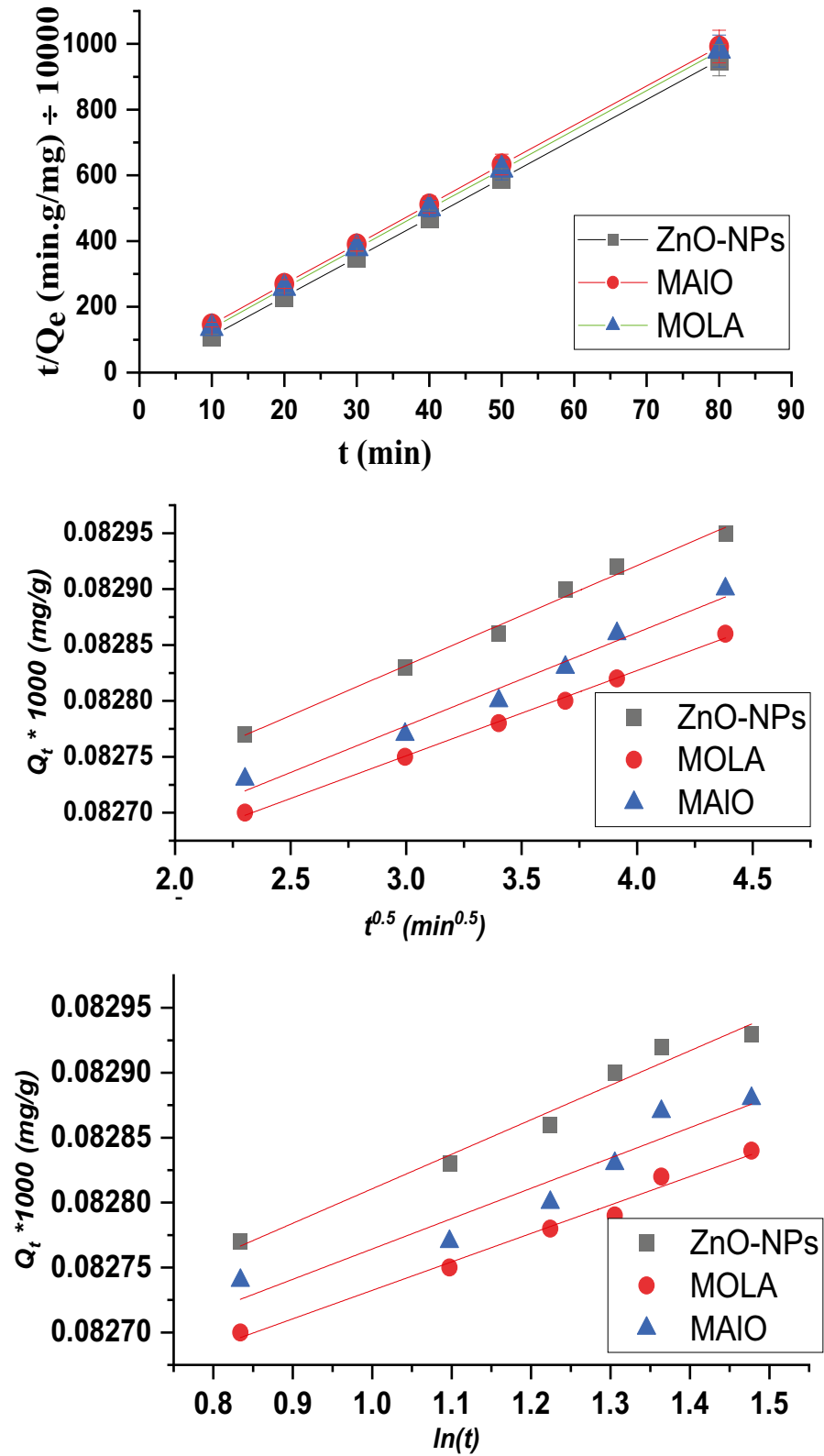
while MOLA has the highest initial adsorption rate and desorption rate. These findings are consistent with the experimental data, which showed that ZnO-NPs adsorbed glyphosate better than MOLA. Hnana et al. (2019) also found that the adsorption of glyphosate obeyed the Elovich model onto ghassoul and chitosan. A similar report, on the use of calcite for the adoption removal of glyphosate from an aqueous medium, also affirmed the suitability of the Elovich equation in the explanation of the adsorption characteristics of the system.

Adsorption isotherms are pivotal in the understanding of the adsorption behaviour of ZnO-NPs, MAlO and MOLA adsorbents. We investigated several isotherms and found that the experimental data fit the Temkin, Freundlich, Brunauer–Emmet–Teller and Dubinin–Radushkevich isotherms (shown in Fig. 6d) gave a better degree of fitness. The listed isotherms were developed based on Eqs. 10, 11 12

and 13, respectively, which represent the assumptions that established them (Brião et al., 2022):

$$ln Q_e = ln k_F + \frac{1}{n} ln C_e \tag{10}$$

$$ln Q_e = \frac{RT}{k_T} ln A_T + \frac{RT}{k_T} ln C_e \tag{11}$$

$$\frac{C_e}{Q_e(C_s - C_e)} = \frac{1}{Q_{m(BET)}C_{BET}} + \frac{(C_{BET} - 1)}{Q_{m(BET)}C_{BET}} \cdot \frac{C_e}{C_s} \tag{12}$$

$$ln Q_e = ln Q_{\max(E)} - \beta \in^2 \tag{13}$$

Equation 6 is the linear equation for the Freundlich isotherm. The consistency of the experimental data with this model was ascertained by the high calculated
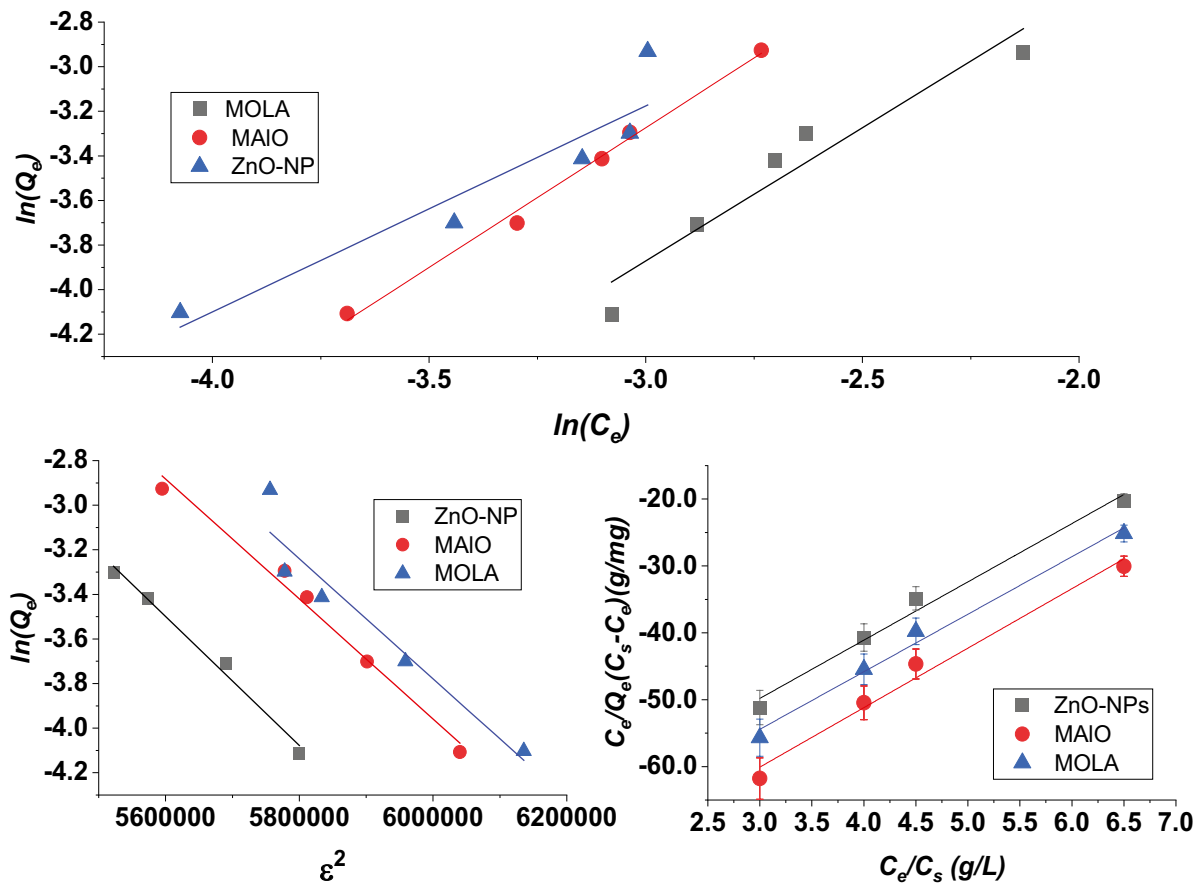

Fig. 6 Freundlich, Temkin, Dubinin–Radushkevich and BET plots for the adsorption of glyphosate by ZnO-NPs, MAlO and MOLA

values of R^2 (Table 2). The adsorption constants of the Freundlich system deduced from the plot (Fig. 6a) were 0.7516, 1.6274 and 0.2418 for ZnO-NPs, MAlO and MOLA (Table 2), respectively. The parameter, $1/n$ (which represents adsorption intensity), energy distribution factor and surface heterogeneity, was less than unity except for MOLA (which had a slight deviation) and therefore confirmed that the adsorption of glyphosate is favourable because $0 < \frac{1}{n} < 1$ (Mahalakshmi et al., 2016). Furthermore, the $1/n$ values are less than unity (except for MOLA), suggesting the favouritism of the physisorption mechanism for ZnO-NP and MALO but the chemisorption mechanism for MOLA (Garg et al., 2022). However, based on the fitness of Elovich and pseudo-second-order kinetic models, it is also inferable that the chemisorption mechanism also features in the adsorption of the pesticides onto ZnO-NP and MAlO but with relatively less dominance. The heterogeneity factor connects the free energy of adsorption ($\Delta G_{ads} = -RTlnk_F$) with the maximum adsorption surface according to Eq. 14 (Eddy et al., 2022a):

$$Q_{max} = \frac{\Delta G_{ads}}{nRT} = \frac{-lnK_F}{n} \qquad (14)$$

The evaluated values of Q_{max} (Table 2) showed that MOLA had the largest unutilized adsorption area, while ZnO-NP had the least, which is also consistent with experimental data.

The Dubinin–Radushkevich plot (a plot of lnQ_e versus ϵ, where $\epsilon = RTln\left(1 + 1/C_e\right)$, expressed in Eq. 9) gave a linear plot with reasonable values of R^2 (Fig. 6). Evaluated values of the Dubinin–Radushkevich adsorption energies ($E = 400$ kJ/mol) (Table 2) for the different adsorbents were less than the maximum required for observing a physical adsorption mechanism. Therefore, based on the Dubinin–Radushkevich data, the adsorption of glyphosate on ZnO-NP and modified ZnO-NP occurred through the mechanism of physicochemical adsorption. However, in their study, Pereira et al. (2019) found a physisorption mechanism for the adsorption of glyphosate onto ferrihydrite using the Dubinin–Radushkevich model.

The BET model (Eq. 14) allows for the occupation of the given adsorption sites by more than one molecule, unlike the Langmuir model which is based on the monolayer of adsorption (Langmuir, 1918). The experimental data did not fit the Langmuir adsorption model but fitted the BET model (because a plot of $\frac{C_e}{Q_e(C_s - C_e)}$ versus $\frac{C_e}{C_s}$ t was linear) as shown in Fig. 6, indicating that there existed a multimolecular layer of adsorption that operated to create a lower adsorption surface (i.e. BET surface), that was almost the same for all the adsorbent (Table 2), where $Q_{m(BET)}$ is the BET monolayer adsorption capacity and C_{BET} is the BET adsorption constant (which followed the trend, ZnO-NP > MAlO > MOLA). Al-Arjan (2022) also affirmed that the BET adsorption isotherm was appropriate in

Table 2 Adsorption parameters for the adsorption of glyphosate by ZnO-NPs, MAlO and MOLA

Adsorption model	ZnO-NP	MAlO	MOLA
Freundlich			
R^2	0.9242	0.9937	0.9871
1/n	1.1952	1.253	0.6569
n	0.8367	0.7981	1.5223
K_f	0.7516	1.6274	0.2418
Q_{max}(mg.g^{-1})	719.467	1226.82	3576.42
Dubinin–Radushkevich			
R^2	0.988	0.9234	0.9862
Q_{max}(mg/g)	3.00E-06	3.00E-06	3.00E-06
β	327,747.9	237,993.8	194,852.9
E_{ads}(KJ/mol)	4.08E+02	4.08E+02	4.08E+02
Brunauer–Emmet–Teller(BET)			
R^2	0.8903	0.8916	0.8921
$Q_{m(BET)}$ (mg/g)	0.00111	0.00112	0.0011
C_{BET}	10.4176	10.3666	10.3067

the explanation of the adsorption of glyphosate by oil palm front. Also, the fitness of the BET isotherm was affirmed by Rodrigues et al. (2023) for the adsorption of glyphosate by palygorskite. Such levels of fitness is an indication of a multiple adsorption layer which is a descriptive term for the adsorption of more than one molecule of glyphosate by a given adsorption site in the ZnO-NPs.

Regeneration study

The three adsorptions were investigated for their reusability (in the re-adsorption of the glyphosate) after washing with distilled water (severally) and drying in the oven. According to the findings, ZnO-NP had the highest reusability index (94.34%), followed by alumina (92.6%) and MOLA (91.65%).

Computational chemistry consideration

Calculated values of semiempirical parameters for glyphosate were $E_{HOMO} = -6.84$ eV, $E_{LUMO} = -1.22$ eV, the energy gap ($\Delta E = E_{LUMO} - E_{HOMO} = 5.62$ eV), dipole moment (7.80 Debye), total energy (-930.6525 au), area (200.08 Å^2), polar surface area (112. 480 Å^2), ovality (1.42) and polarizability (53.84 Å^3). The HOMO and LUMO parameters can effectively be represented through a molecular surface plot, which is shown in Fig. 7a for glyphosate (Ebenso et al., 2021). The positive charge (red) is seen to concentrate on the heteroatom, while the
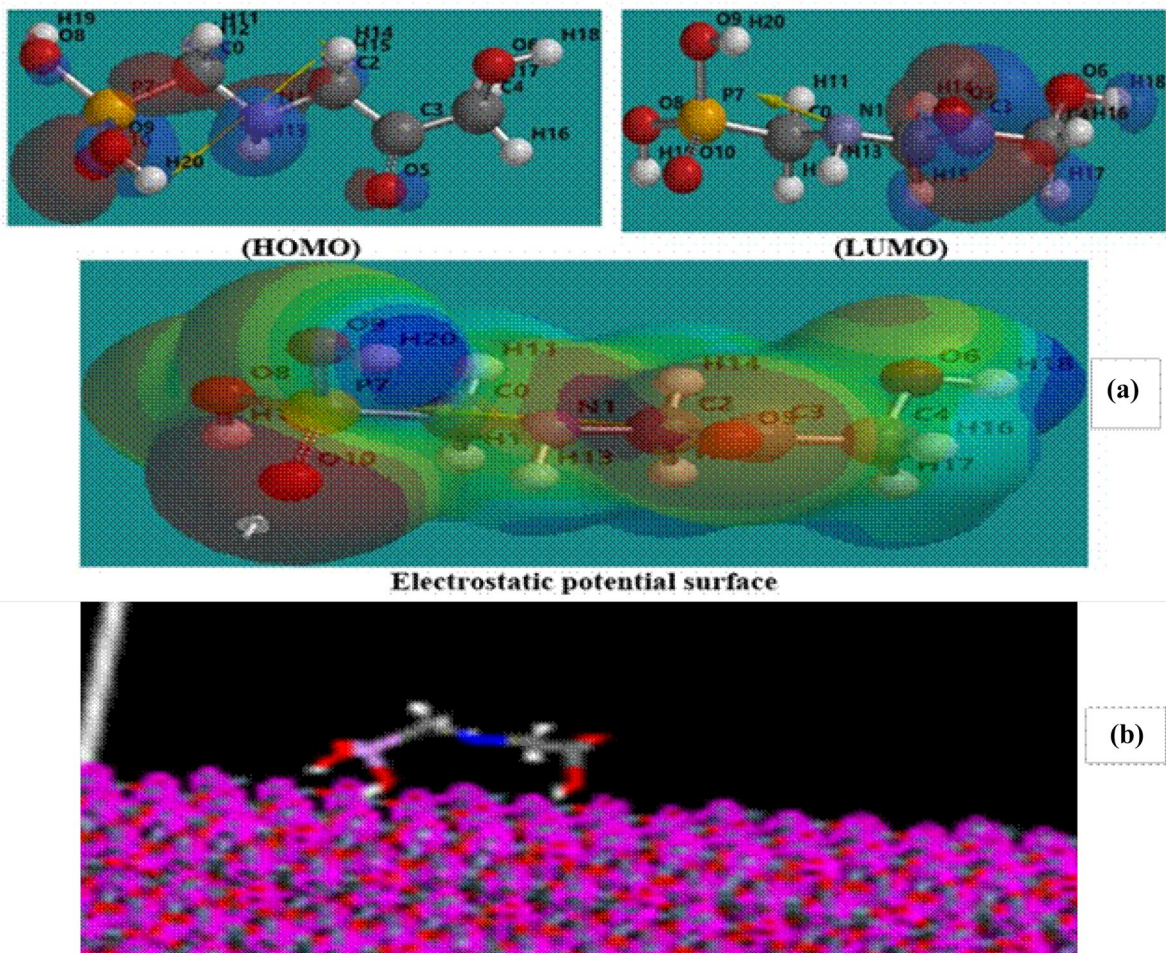

Fig. 7 a Surfaces showing the HOMO and LUMO locations in glyphosate. **b** Adsorption interaction model between glyphosate and ZnO-NPs

negative lobes concentrate on the carbon atoms. Figure 6a also shows the electrostatic potential plot (ESP) for glyphosate which reveals different ESP surfaces as shown by differences in colour.

The fundamental of the semiempirical calculations is that molecular reactivity is addressed as a global property without consideration of the contributions from each of the participating atoms in a molecule. Local reactivity can be addressed by the charges on each atom, but the most formal approach involves the calculation of Fukui functions, which can be defined as a process involving the loss of electron $(N-1)$, the gain of electron $(N+1)$ and neutral state (N). The first Fukui function defines electrophilic (Eq. 16), the second nucleophilic (Eq. 15) and the last radical Fukui functions (Eq. 17) (Eddy & Ameh, 2021):

$$f_x^+ = q_{N+1} - q_N \tag{15}$$

$$f_x^- = q_N - q_{N-1} \tag{16}$$

$$f_x^0 = \frac{(q_{N+1} - q_{N-1})}{2} \tag{17}$$

The functionality of the above equations is the assignment of the sites with the highest positive values of the Fukui functions as the appropriate functional atom or bonds. Therefore, based on the calculated Fukui functions, the sites for electrophilic, nucleophilic and radical attacks are on the preference of O(11) atom, C(4)-O(6) bond and O(6) atom, respectively. The Fukui functions were evaluated using Mulliken and Hirshfeld charges for $N+1$ (q_{N+1}), $N-1$ (q_{N-1}) and N (q_N) electronic systems. Quantum chemical investigation was also extended to cover the adsorption-associated interaction energy through Monte Carlo simulation modelling using the adsorption locator program in the Materials Studio software (see Fig. 7b). The adsorption locator function indicated that the insecticide is adsorbed on the surface of zinc oxide nanoparticles, which are also consistent with the findings from the evaluated Fukui functions.

The total energy, adsorption energy (E_{ads}), rigid adsorption energy, deformation energy and $\frac{dE_{ads}}{dN}$ were evaluated to correspond to $-27.9913, -56.5196, -62.4737, 5.9541$ and -56.5196 kcal/mol, respectively. The negative value of the E_{ads} confirms the exothermic adsorption process (between the pesticide and the ZnO-NPs) resulting from the decrease in surface energy as the glyphosate molecules approach the surface of the adsorbent. The evaluated adsorption energy $(-56.5196$ kJ/mol) is consistent with the range of data expected for the mechanism of chemisorption adsorption (i.e. $200 > E_{ads}$ (kJ/mol). Therefore, the adsorption of glyphosate on the nanosurface first responded to the physical adsorption and was succeeded by the chemisorption mechanism (Eddy et al., 2018). The sum of the deformation (5.9541 kcal/mol) and rigid adsorption energy $(-62.4737$ kcal/mol) is the equivalent of the E_{ads}. The rigid energy component is associated with the energy released when the unrelaxed glyphosate is adsorbed on the surface of the ZnO nanoparticles, while the energy released when the adsorbed molecule is relaxed on the surface is the deformation energy. Also, since the total energy is the sum of the internal and adsorption energy, then, the calculated internal energy of the adsorbed system is equal to 84.5109 kcal/mol (Yuan et al., 2005).

Conclusions

ZnO-NPs with wurtzite crystalline structure have been synthesized by the application of the precipitation method. The produced nanoparticles showed major FTIR peaks at 459 nm and a ZnO stretching are typical ZnO-NPs. Apart from the reduction in crystallite sizes, modification of the adsorbent by alumina and oleic acid (+ xylene) resulted in a more ordered crystal but with an increased amorphous character. The synthesized ZnO-NPs, MAlO and MOLA are good adsorbents for the removal of glyphosate from an aqueous medium. The adsorption tends to be dominated by a chemical adsorption mechanism, showing excellent fitness for pseudo-second-order kinetics. The present results showed that more than 90% glyphosate can be withdrawn from aqueous media through adsorption by the zinc oxide nanoparticles and the modified samples.

Author contribution Steven A. Odoemelam: conceptualization, investigation and writing, original draft; Esther O. Oji: formal analysis, methodology and writing, original draft; Nnabuk

Declarations

All authors have read, understood and have complied as applicable with the statement on "Ethical responsibilities of authors" as found in the Instructions for Authors and are aware that with minor exceptions, no changes can be made to authorship once the paper is submitted.

Ethics approval Not applicable.

Consent to participate Not applicable.

Consent for publication Not applicable.

Competing interests The authors declare no competing interests.

References

Al-Arjan, W. S. (2022). Zinc oxide nanoparticles and their application in adsorption of toxic dye from aqueous solution. *Polymers*, *14*(15). https://doi.org/10.3390/polym14153086

Al-Harby, N. F., Albahly, E. F., & Mohamed, N. A. (2021). Kinetics, isotherm and thermodynamic studies for efficient adsorption of Congo red dye from aqueous solution onto novel cyanoguanidine-modified chitosan adsorbent. *Polymers*, *13*(24). https://doi.org/10.3390/polym13244446

Ali, M., Prakash, K., Macana, C., Bashir, A. K., Jolfaei, A., Bokhari, A., et al. (2022). Modeling residential electricity consumption from public demographic data for sustainable cities. *Energies, 15*(6), 1–16. https://doi.org/10.3390/en15062163

An, B., Lee, C. G., Song, M. K., Ryu, J. C., Lee, S., Park, S. J., et al. (2015). Applicability and toxicity evaluation of an adsorbent based on jujube for the removal of toxic heavy metals. *Reactive and Functional Polymers, 93*, 138–147. https://doi.org/10.1016/j.reactfunctpolym.2015.06.009

Babapour, M., Hadi Dehghani, M., Alimohammadi, M., Moghadam Arjmand, M., Salari, M., Rasuli, L., et al. (2022). Adsorption of Cr(VI) from aqueous solution using mesoporous metal-organic framework-5 functionalized with the amino acids:

Characterization, optimization, linear and nonlinear kinetic models. *Journal of Molecular Liquids*, *345*, 117835. https://doi.org/10.1016/j.molliq.2021.117835

Barbosa, L. M. S., Baêta, B. E. L., de Barros, A. L. C., Braga Almeida, M. L., & Libânio, M. (2023). Sugarcane bagasse ash for fipronil removal. *Water Practice and Technology, 18*(1), 231–242. https://doi.org/10.2166/wpt.2022.174

Bazan-Wozniak, A., & Pietrzak, R. (2023). Adsorption of cationic dye on nanostructured biocarbons: Kinetic and thermodynamic study. *Applied Nanoscience (Switzerland)*, (0123456789). https://doi.org/10.1007/s13204-023-02775-9

Brião, G. de V., da Silva, M. G. C., Vieira, M. G. A., & Chu, K. H. (2022). Correlation of type II adsorption isotherms of water contaminants using modified BET equations. *Colloids and Interface Science Communications*, *46*. https://doi.org/10.1016/j.colcom.2021.100557

Caixeta, M. P. (2023). Contaminants of emerging concern: A review of risk assessment and treatment strategies. *U.Porto Journal of Engineering*, *9*(1), 191–228. https://doi.org/10.24840/2183-6493_009-001_001282

Chen, F., & xiong, Zhou, C. rong, Li, G. peng, & Peng, F. fei. (2016). Thermodynamics and kinetics of glyphosate adsorption on resin D301. *Arabian Journal of Chemistry, 9*, S1665–S1669. https://doi.org/10.1016/j.arabjc.2012.04.014

Cosgrove, S., Jefferson, B., & Jarvis, P. (2022). Application of activated carbon fabric for the removal of a recalcitrant pesticide from agricultural run-off. *Science of the Total Environment*, *815*, 152626. https://doi.org/10.1016/j.scitotenv.2021.152626

Da'ana, D. A., Zouari, N., Ashfaq, M. Y., Abu-Dieyeh, M., Khraisheh, M., Hijji, Y. M., & Al-Ghouti, M. A. (2021). Removal of toxic elements and microbial contaminants from groundwater using low-cost treatment options. *Current Pollution Reports, 7*(3), 300–324. https://doi.org/10.1007/s40726-021-00187-3

Dangana, R. S., George, R. C., & Agboola, F. K. (2023). The biosynthesis of zinc oxide nanoparticles using aqueous leaf extracts of Cnidoscolus aconitifolius and their biological activities. *Green Chemistry Letters and Reviews*, *16*(1). https://doi.org/10.1080/17518253.2023.2169591

Diel, J. C., da Boit Martinello, K., da Silveira, C. L., Pereira, H. A., Franco, D. S. P., Silva, L. F. O., & Dotto, G. L. (2022). New insights into glyphosate adsorption on modified carbon nanotubes via green synthesis: Statistical physical modeling and steric and energetic interpretations. *Chemical Engineering Journal*, *431*, 134095. https://doi.org/10.1016/j.cej.2021.134095

Ebenso, E. E., Verma, C., Olasunkanmi, L. O., Akpan, E. D., Verma, D. K., Lgaz, H., et al. (2021). Molecular modelling of compounds used for corrosion inhibition studies: A review. *Physical Chemistry Chemical Physics: PCCP*, *23*(36), 19987–20027. https://doi.org/10.1039/D1CP00244A

Eddy, N. O., & Ameh, P. O. (2021). Computational and experimental study on Tapinanthus bangwensis leaves as corrosion inhibitor for mild steel and Al in 0.1 M HCl. *Current Topics in Electrochemistry, 23*, 45–62.

Eddy, N. O., Ameh, P. O., & Essien, N. B. (2018). Experimental and computational chemistry studies on the inhibition of aluminium and mild steel in 0.1 M HCl by 3-nitrobenzoic acid. *Journal of Taibah University for Science*, *12*(5), 545–556. https://doi.org/10.1080/16583655.2018.1500514

Eddy, N. O., Garg, R., Garg, R., Aikoye, A. O., & Ita, B. I. (2022a). Waste to resource recovery: Mesoporous adsorbent from orange peel for the removal of trypan blue dye from aqueous solution. *Biomass Conversion and Biorefinery*. https://doi.org/10.1007/s13399-022-02571-5

Eddy, N. O., Odoemelam, S. A., Ogoko, E. C., Ukpe, R. A., Garg, R., & Anand, B. (2022b). Experimental and quantum chemical studies of synergistic enhancement of the corrosion inhibition efficiency of ethanol extract of Carica papaya peel for aluminum in solution of HCl. *Results in Chemistry*, *4*. https://doi.org/10.1016/j.rechem.2022.100290

Eddy, N. O., Ukpe, R. A., Ameh, P., Ogbodo, R., Garg, R., & Garg, R. (2022c). Theoretical and experimental studies on photocatalytic removal of methylene blue (MetB) from aqueous solution using oyster shell synthesized CaO nanoparticles (CaONP-O). *Environmental Science and Pollution Research*. https://doi.org/10.1007/s11356-022-22747-w

Egbuchunam, T., & Balkose, D. (2012). Effect of supercritical ethanol drying on the properties of zinc oxide nanoparticles. *Drying Technology, 30*(7), 739–749. https://doi.org/10.1080/07373937.2012.661380

Elfeky, A. S., Youssef, H. F., & Elzaref, A. S. (2020). Adsorption of dye from wastewater onto ZnO nanoparticles-loaded zeolite: Kinetic, thermodynamic and isotherm studies. *Zeitschrift Fur Physikalische Chemie, 234*(2), 255–278. https://doi.org/10.1515/zpch-2018-1342

Garg, R., Rani, P., Garg, R., & Eddy, N. O. (2021). Study on potential applications and toxicity analysis of green synthesized nanoparticles. *Turkish Journal of Chemistry, 45*(6), 1690–1706. https://doi.org/10.3906/kim-2106-59

Garg, Rishav, Garg, R., Okon Eddy, N., Ibrahim Almohana, A., Fahad Almojil, S., Amir Khan, M., & Ho Hong, S. (2022). Biosynthesized silica-based zinc oxide nanocomposites for the sequestration of heavy metal ions from aqueous solutions. *Journal of King Saud University - Science, 34*(4), 101996. https://doi.org/10.1016/j.jksus.2022.101996

Ghavamifar, S., Naidu, R., Mozafari, V., & Li, Z. (2023). Can calcite play a role in the adsorption of glyphosate? A comparative study with a new challenge. *Chemosphere*, *311*, 136922. https://doi.org/10.1016/j.chemosphere.2022.136922

Gkika, D. A., Mitropoulos, A. C., & Kyzas, G. Z. (2022). Why reuse spent adsorbents? The latest challenges and limitations. *Science of the Total Environment*, *822*, 153612. https://doi.org/10.1016/j.scitotenv.2022.153612

Gogoi, H., Mani, R., Aggarwal, S., Malik, A., Munde, M., & Bhatnagar, R. (2020). Crystalline and amorphous preparation of aluminum hydroxide nanoparticles enhances protective antigen domain 4 specific immunogenicity and provides protection against anthrax. *International Journal of Nanomedicine, 15*, 239–252. https://doi.org/10.2147/IJN.S219647

Hagner, M., Mikola, J., Saloniemi, I., Saikkonen, K., & Helander, M. (2019). Effects of a glyphosate-based herbicide on soil animal trophic groups and associated ecosystem functioning in a northern agricultural field. *Scientific Reports, 9*(1), 1–13. https://doi.org/10.1038/s41598-019-44988-5

Handore, K., Bhavsar, S., Horne, A., Chhattise, P., Mohite, K., Ambekar, J., et al. (2014). Novel green route of synthesis of ZnO nanoparticles by using natural biodegradable polymer and its application as a catalyst for oxidation of aldehydes. *Journal of Macromolecular Science, Part A, 51*(12), 941–947. https://doi.org/10.1080/10601325.2014.967078

Hnana, K., Barhoun, A., & Draoui, K. (2019). Improvement of glyphosate adsorption using new composites based on ghassoul and chitosan: Kinetics and equilibrium study. *Mediterranean Journal of Chemistry, 9*(4), 266–279. https://doi.org/10.13171/mjc9419111121087kd

Hong, R., Pan, T., Qian, J., & Li, H. (2006). Synthesis and surface modification of ZnO nanoparticles. *Chemical Engineering Journal, 119*(2–3), 71–81. https://doi.org/10.1016/j.cej.2006.03.003

Hong, T., Yin, J.-Y., Nie, S.-P., & Xie, M.-Y. (2021). Applications of infrared spectroscopy in polysaccharide structural analysis: Progress, challenge and perspective. *Food Chemistry: X, 12*, 100168. https://doi.org/10.1016/j.fochx.2021.100168

Hosseini, N., & Toosi, M. R. (2019). Removal of 2,4-D, glyphosate, trifluralin, and butachlor herbicides from water by polysulfone membranes mixed by graphene oxide/TiO2 nanocomposite: Study of filtration and batch adsorption. *Journal of Environmental Health Science and Engineering, 17*(1), 247–258. https://doi.org/10.1007/s40201-019-00344-3

Hubbe, M. A. (2022). What-to-do-with-toxic-contaminated-cellulosebased-adsorbents_2022_North-Carolina-State-University. *BioResources, 17*(1), 3–6.

Jia, D., Zhou, C., & Li, C. (2011). Adsorption of glyphosate on resin supported by hydrated iron oxide: Equilibrium and kinetic studies. *Water Environment Research, 83*(9), 784–790. https://doi.org/10.1002/j.1554-7531.2011.tb00268.x

Kaczorowska, M. A., Bożejewicz, D., & Witt, K. (2023). The application of polymer inclusion membranes for the removal of emerging contaminants and synthetic dyes from aqueous solutions—A mini review. *Membranes*, *13*(2). https://doi.org/10.3390/membranes13020132

Kalsoom, Khan, S., Ullah, R., Adil, M., Waheed, A., Khan, K. A., et al. (2022). Adsorption of pesticides using wood-derived biochar and granular activated carbon in a fixed-bed column system. *Water (Switzerland)*, *14*(19). https://doi.org/10.3390/w14192937

Kamal, A., Saba, M., Ullah, K., Almutairi, S. M., AlMunqedhi, B. M., & Ragab abdelGawwad, M. (2023). Mycosynthesis, characterization of zinc oxide nanoparticles, and its assessment in various biological activities. *Crystals, 13*(2). https://doi.org/10.3390/cryst13020171

Khoshhesab, Z. M., Sarfaraz, M., & Asadabad, M. A. (2011). Preparation of ZnO nanostructures by chemical precipitation method. *Synthesis and Reactivity in Inorganic, Metal-Organic and Nano-Metal Chemistry, 41*(7), 814–819. https://doi.org/10.1080/15533174.2011.591308

Kumar, A., Yu, Z.-G., Klemeš, J. J., & Bokhari, A. (2021). A state-of-the-art review of greenhouse gas emissions from Indian hydropower reservoirs. *Journal of Cleaner Production, 320*, 128806. https://doi.org/10.1016/j.jclepro.2021.128806

Langmuir, I. (1918). The adsorption of gases on plane surfaces of glass, mica and platinum. *Journal of the American Chemical Society, 40*(9), 1361–1403. https://doi.org/10.1021/ja02242a004

Maderthaner, M., Weber, M., Takács, E., Mörtl, M., Leisch, F., Römbke, J., et al. (2020). Commercial glyphosate-based herbicides effects on springtails (Collembola) differ from those of their respective active ingredients and vary with soil organic matter content. *Environmental Science and Pollution Research, 27*(14), 17280–17289. https://doi.org/10.1007/s11356-020-08213-5

Mahalakshmi, K., Nithya, R., & Nithyananthi, M. J. T. (2016). Adsorption and inhibitive properties of ethanol extracts of Acacia nilotica as a green corrosion inhibitor for mild steel in acidic media. *Journal of Chemical and Pharmaceutical Sciences, 9*(1), 196–201.

Mattos, R., Khan, S., Hussain, S., & De Alencar Simoni, J. (2017). Quantitation and adsorption of glyphosate using various treated clay. *Zeitschrift Fur Physikalische Chemie, 231*(11–12), 1815–1829. https://doi.org/10.1515/zpch-2016-0942

Mazari, S. A., Ali, E., Abro, R., Khan, F. S. A., Ahmed, I., Ahmed, M., et al. (2021). Nanomaterials: Applications, waste-handling, environmental toxicities, and future challenges – A review. *Journal of Environmental Chemical Engineering*, *9*(2), 105028. https://doi.org/10.1016/j.jece.2021.105028

Mohan, A. C., & Renjanadevi, B. (2016). Preparation of zinc oxide nanoparticles and its characterization using scanning electron microscopy (SEM) and X-ray diffraction (XRD). *Procedia Technology, 24*, 761–766. https://doi.org/10.1016/j.protcy.2016.05.078

Naghdi, S., Brown, E., Zendehbad, M., Duong, A., Ipsmiller, W., Biswas, S., et al. (2023). Glyphosate adsorption from water using hierarchically porous metal–organic frameworks. *Advanced Functional Materials*, *2213862*. https://doi.org/10.1002/adfm.202213862

Odoemelam, S. A., Emeh, U. N., & Eddy, N. O. (2018). Experimental and computational chemistry studies on the removal of methylene blue and malachite green dyes from aqueous solution by neem (Azadirachta indica) leaves. *Journal of Taibah University for Science, 12*(3), 255–265. https://doi.org/10.1080/16583655.2018.1465725

Páez, M. R., Ochoa-Muñoz, Y., & Rodriguez-Páez, J. E. (2019). Efficient removal of a glyphosate-based herbicide from water using ZnO nanoparticles (ZnO-NPs). *Biocatalysis and Agricultural Biotechnology*, *22*, 101434. https://doi.org/10.1016/j.bcab.2019.101434

Peillex, C., & Pelletier, M. (2020). The impact and toxicity of glyphosate and glyphosate-based herbicides on health and immunity. *Journal of Immunotoxicology, 17*(1), 163–174. https://doi.org/10.1080/1547691X.2020.1804492

Pelicano, C. M., Rapadas, N. J., & Magdaluyo, E. (2017). X-ray peak profile analysis of zinc oxide nanoparticles formed by simple precipitation method. *AIP Conference Proceedings, 1901*(1), 20016. https://doi.org/10.1063/1.5010453

Peng, G., Tang, B., & Zhou, X. (2021). Effect of preparation methods on the adsorption of glyphosate by calcined Ca-Al hydrotalcite. *ACS Omega, 6*(24), 15742–15749. https://doi.org/10.1021/acsomega.1c01025

Pereira, R. C., Anizelli, P. R., Di Mauro, E., Valezi, D. F., Da Costa, A. C. S., Zaia, C. T. B. V., & Zaia, D. A. M. (2019). The effect of pH and ionic strength on the adsorption of glyphosate onto ferrihydrite. *Geochemical Transactions, 20*(1), 1–14. https://doi.org/10.1186/s12932-019-0063-1

Pérez-Lucas, G., Aatik, A. El, Aliste, M., Navarro, G., Fenoll, J., & Navarro, S. (2023). Removal of contaminants of emerging concern from a wastewater effluent by solar-driven heterogeneous photocatalysis: A case study of pharmaceuticals. *Water, Air, and Soil Pollution*, *234*(1). https://doi.org/10.1007/s11270-023-06075-4

Rápó, E., & Tonk, S. (2021). Factors affecting synthetic dye adsorption; desorption studies: A review of results from the last five years (2017–2021). *Molecules*, *26*(17). https://doi.org/10.3390/molecules26175419

Rodrigues, P. V., Silva, F. A. N. G., Pontes, F. V. M., Barbato, C. N., Teixeira, V. G., Assis, T. C. de, et al. (2023). Adsorption of glyphosate by palygorskite. *Materials Research*, *26*. https://doi.org/10.1590/1980-5373-mr-2022-0335

Sedighi, M., Behvand Usefi, M. M., Ismail, A. F., & Ghasemi, M. (2023). Environmental sustainability and ions removal through electrodialysis desalination: Operating conditions and process parameters. *Desalination*, *549*, 116319. https://doi.org/10.1016/j.desal.2022.116319

Sen, K., & Mondal, N. K. (2022). Glyphosate adsorptive behaviour using magnetic activated carbon: Kinetics, isotherms, and DFT study. *Biomass Conversion and Biorefinery*. https://doi.org/10.1007/s13399-021-02193-3

Silva, C. E. de F., Gama, B. M. V. da, Gonçalves, A. H. da S., Medeiros, J. A., & Abud, A. K. de S. (2020). Basic-dye adsorption in albedo residue: Effect of pH, contact time, temperature, dye concentration, biomass dosage, rotation and ionic strength. *Journal of King Saud University - Engineering Sciences*, *32*(6), 351–359. https://doi.org/10.1016/j.jksues.2019.04.006

Silva, M., Eisa, M., Ragauskaitė, D., McMinn, M. H., Tian, Z., Williams, C., et al. (2023). Treatment of emerging contaminants in simulated wastewater via tandem photo-Fenton-like reaction and nutrient recovery. *Environ. Sci.: Water Res. Technol.*, *9*(2), 508–522. https://doi.org/10.1039/D2EW00209D

Tarazona, J. V., Court-Marques, D., Tiramani, M., Reich, H., Pfeil, R., Istace, F., & Crivellente, F. (2017). Glyphosate toxicity and carcinogenicity: A review of the scientific basis of the European Union assessment and its differences with IARC. *Archives of Toxicology, 91*(8), 2723–2743. https://doi.org/10.1007/s00204-017-1962-5

Tiwari, A. K., Jha, S., Singh, A. K., Mishra, S. K., Pathak, A. K., Ojha, R. P., et al. (2022). Innovative investigation of zinc oxide nanoparticles used in dentistry. *Crystals*, *12*(8). https://doi.org/10.3390/cryst12081063

Warren-Vega, W. M., Campos-Rodríguez, A., Zárate-Guzmán, A. I., & Romero-Cano, L. A. (2023). A current review of water pollutants in american continent: Trends and perspectives in detection, health risks, and treatment technologies. *International journal of environmental research and public health*, *20*(5). https://doi.org/10.3390/ijerph20054499

Xin, M. (2022). Crystal structure and optical properties of ZnO: Ce nano film. *Molecules, 27*(16), 1–9. https://doi.org/10.3390/molecules27165308

Xu, H., Wang, B., Zhao, R., Wang, X., Pan, C., Jiang, Y., et al. (2022). Adsorption behavior and performance of ammonium onto sorghum straw biochar from water. *Scientific Reports, 12*(1), 1–12. https://doi.org/10.1038/s41598-022-08591-5

Yuan, F., Peng, H., Yin, Y., Chunlei, Y., & Ryu, H. (2005). Preparation of zinc oxide nanoparticles coated with homogeneous Al 2O3 layer. *Materials Science and Engineering B: Solid-State Materials for Advanced Technology, 122*(1), 55–60. https://doi.org/10.1016/j.mseb.2005.04.016

Zahmatkesh, S., Bokhari, A., Karimian, M., Zahra, M. M. A., Sillanpää, M., Panchal, H., et al. (2022). A comprehensive review of various approaches for treatment of tertiary wastewater with emerging contaminants: What do we know?

Environmental Monitoring and Assessment, 194(12), 884. https://doi.org/10.1007/s10661-022-10503-z

Zhao, M., Zhang, J., Wang, W., & Zhang, Q. (2021). High effective preparation of amorphous-like si nanoparticles using spark erosion followed by bead milling. *Nanomaterials (Basel, Switzerland), 11*(3). https://doi.org/10.3390/nano11030594

Zhou, C., Jia, D., Liu, M., Liu, X., & Li, C. (2017). Removal of glyphosate from aqueous solution using nanosized copper hydroxide modified resin: Equilibrium isotherms and kinetics. *Journal of Chemical and Engineering Data, 62*(10), 3585–3592. https://doi.org/10.1021/acs.jced.7b00569